

# Fuse the $\pi$ -Bridge to Acceptor Moiety of Donor- $\pi$ -Acceptor Conjugated Polymer: Enabling an All-Round Enhancement in Photovoltaic Parameters of Nonfullerene Organic Solar Cells


Lu Yu,<sup>†,‡</sup> Yonghai Li,<sup>\*,‡</sup> Yuancheng Wang,<sup>§</sup> Xunchang Wang,<sup>‡</sup> Wen Cui,<sup>†</sup> Shuguang Wen,<sup>‡</sup> Nan Zheng,<sup>\*,||</sup> Mingliang Sun,<sup>\*,‡</sup> and Renqiang Yang<sup>\*,‡</sup>

<sup>†</sup>School of Materials Science and Engineering, Ocean University of China, Qingdao 266100, China

<sup>‡</sup>CAS Key Laboratory of Bio-Based Materials, Qingdao Institute of Bioenergy and Bioprocess Technology, Chinese Academy of Sciences, Qingdao 266101, China

<sup>§</sup>School of Polymer Science and Engineering, Qingdao University of Science and Technology, Qingdao 266042, China

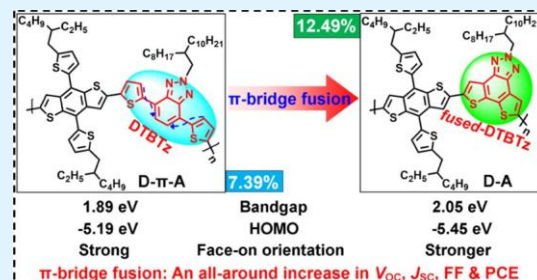
<sup>||</sup>State Key Laboratory of Luminescent Materials and Devices, South China University of Technology, Guangzhou 510640, China

 Supporting Information

**ABSTRACT:** The D- $\pi$ -A conjugated polymers with a benzotriazole (BTz) unit as the A moiety have been intensively investigated as donor materials in nonfullerene solar cells. However, these BTz even the fluorinated-BTz constructed D- $\pi$ -A polymers mostly suffered from upward highest occupied molecular orbital (HOMO) energy levels, leading to inferior open-circuit voltage ( $V_{OC}$ ) and efficiencies in the fabricated solar cells. Herein, we explored a new approach in response to this issue via the strategy of  $\pi$ -bridge fusion to A moiety. As a result, the medium band gap D- $\pi$ -A polymer PY2 was evolved into wide band gap D-A polymer PY1 with fused-DTBTz as the new A moiety, accompanied with a greatly declined HOMO energy level by 0.26 eV,

a remarkable blue-shifted absorption onset by about 51 nm, and concurrently moderately enhanced face-on stacking orientations in neat polymer and donor/acceptor blend films. The synergetic optimizations in energy level, absorption characteristic and molecular stacking feature via the  $\pi$ -bridge fusion design witness an all-round improvement in photovoltaic parameters including the focused  $V_{OC}$ , short-circuit current density ( $J_{SC}$ ), and fill factor (FF), with narrow band gap ITIC as the acceptor material. Specifically, the PY1-based solar cells produce an optimal power conversion efficiency (PCE) of 12.49%, with superior  $V_{OC}$  of 0.94 V,  $J_{SC}$  of 18.46 mA cm<sup>-2</sup>, and FF of 0.72, significantly surpassing those of PY2-based optimal device with a PCE of 7.39%,  $V_{OC}$  of 0.77 V,  $J_{SC}$  of 14.54 mA cm<sup>-2</sup>, and FF of 0.66 and even the reported classical fluorinated-BTz based polymer J51 ( $V_{OC}$  of 0.82 V, PCE of 9.26%). Promisingly, there is a huge room for improvement in photovoltaic properties with rational fluorination or chlorination of the fused-DTBTz unit or the D moiety of the D-A polymers.

**KEYWORDS:** donor- $\pi$ -acceptor, conjugated polymers,  $\pi$ -bridge fusion, photovoltaic properties, organic solar cells



## INTRODUCTION

Bulk-heterojunction organic solar cells (BHJ-OSCs) have attracted increasing attention as a future green power technology to utilize the inexhaustible solar energy owing to their great potential for low cost, light weight, easy fabrication, and flexibility.<sup>1–3</sup> The development of OSCs has been heavily dragged behind for a long time that is ascribed to the narrow, intractable absorption profiles of traditional fullerene acceptors which undoubtedly limit the harvest of solar energy.<sup>4–6</sup> To maximize the short-circuit current densities ( $J_{SC}$ ) which are closely associated with the light-harvesting properties of BHJ blends, narrow band gap polymeric donors were developed to enlarge the absorption range promoting the power conversion efficiencies over 11%.<sup>7</sup> Nevertheless, restricted by the fixed frontier energy levels of fullerene acceptors and the prerequisite offset of energy levels between the donor and

fullerene acceptor, the band gaps of most efficient donor materials (PTB7, PTB7-Th, PNTz4T, for instance) are often greater than 1.60 eV with the absorption onset lower than 800 nm.<sup>8–10</sup> To overcome these challenges, researchers are exploring the potentials of nonfullerene acceptors with easy-tuning energy levels and absorption properties. Among them, fused-ring acceptor-donor-acceptor (A-D-A) molecule ITIC and its analogues are the most promising nonfullerene acceptors for the state-of-the-art OSCs, which enhances the development of OSCs with on-going exciting breakthroughs in single and tandem solar cells.<sup>11–19</sup> Different from the traditional fullerene acceptors, the absorption properties of

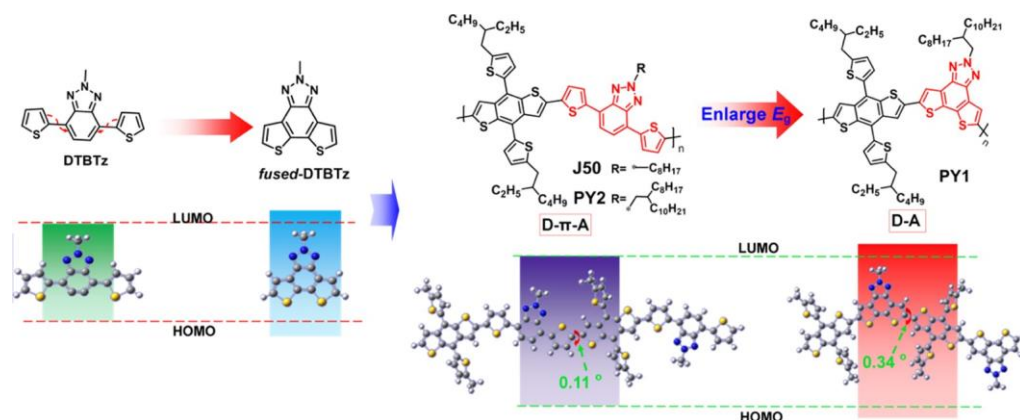
Received: May 31, 2019

Accepted: August 2, 2019

Published: August 2, 2019



Scheme 1. Molecular Structures and Conformations of Units DTBTz, Fused-DTBTz, and the Corresponding Polymer PY2 (J50) and PY1



fused-ring nonfullerene acceptors can be easily broadened to the near-infrared region exceeding 800 nm. Thus, wide band gap polymeric donors are particularly favored in nonfullerene OSCs (NFOSCs) to match the narrow band gap acceptors, generating strong and broad photoresponse spectra.

Benzotriazole (BTz) moiety is one of the widely adopted A unit for the design of wide/medium band gap D- $\pi$ -A polymers, owing to its relatively weak electron-deficient feature and feasible modification of functional substitutions. Based on BTz and fluorinated-BTz units, a series of efficient medium band gap benzodithiophene- $\pi$ -benzotriazole (BDT- $\pi$ -BTz) copolymers (J50, J51, J61, J71, FTAZ, etc.) have been reported in NFOSCs.<sup>20–25</sup> It is noteworthy that most of the BDT- $\pi$ -BTz polymers with decent photovoltaic efficiencies are constructed from the fluorinated BTz unit. Specifically, FTAZ: IDCIC (optical band gap: 1.45 eV)-based NFOSCs optimized with a binary additive afford an impressive power conversion efficiency (PCE) over 13.5%.<sup>25</sup> The fluorination has been proven effective to produce an ordered crystalline structure for a higher hole mobility through intra- or intermolecular interactions, which is closely related to the enhancement of  $J_{SC}$  and fill factor (FF) of solar cells.<sup>18,26,27</sup> Furthermore, the electronegative effect of the fluorine atom attached to the BTz unit could downshift the highest occupied molecular orbital (HOMO) energy level of the polymer, affording a fair open-circuit voltage ( $V_{OC}$ ) in the resulting OSC.<sup>28,29</sup> Nevertheless, the additional fluorination of BTz could inevitably decrease the solubility of the polymers and sometimes damage the film-forming properties of the materials. However, the  $V_{OC}$  of solar cells from nonfluorinated BTz polymers could be unlikely ascribed to the high-lying HOMO energy levels. For instance, NFOSCs based on J51 (fluorinated BTz) and ITIC delivered a decent PCE of 9.26%, with a  $V_{OC}$  of 0.82 V,  $J_{SC}$  of 16.47 mA cm<sup>-2</sup>, and FF of 0.69. By contrast, the optimized OSCs fabricated from J50 (non-fluorinated BTz) and ITIC afforded a much lower PCE of 4.80% with a  $V_{OC}$  of 0.71 V,  $J_{SC}$  of 12.93 mA cm<sup>-2</sup>, and FF of 0.53.<sup>20</sup> Likewise, similar photovoltaic behaviors were observed in J50 and J51 fabricated all polymer solar cells with N2200 as the polymeric acceptor.<sup>21</sup>

Conventionally, the thiophene group is utilized as the  $\pi$ -bridge for most D- $\pi$ -A conjugated polymers not only to tailor the basic photophysical and electrochemical properties but also to play a critical role to alleviate the intense steric hindrance between the bulky D and A moieties and to increase

the planarity of polymer backbones.<sup>30–32</sup> The same goes for BDT- $\pi$ -BTz-based polymers. From another perspective, the thiophene-BTz combination could also be considered as a whole (named as DTBTz) featured as an electron-withdrawing unit. Based on this point, the BDT- $\pi$ -BTz based D- $\pi$ -A conjugated polymer could be regarded as BDT-DTBTz-constructed D-A conjugated polymer. However, the rotatable  $\sigma$ -bond between thiophene and BTz could influence the planarity of polymer backbones.

Hereon, we tactically dismiss the  $\pi$ -bridge and fuse it to the A unit (BTz) and present a different electron-deficient unit labeled as fused-DTBTz in this work (see Scheme 1). Although the structure of the fused-DTBTz has been previously reported in synthetic methodology, it has never been utilized in the OSCs.<sup>33</sup> With DTBTz and fused-DTBTz as the A units, two corresponding conjugated polymers PY2 (or J50) and PY1 were reported. The results indicate that the fusion of the  $\pi$ -bridge to A moiety does not disturb the planarity of the polymer backbone and face-on orientations which is gratifying and essential to keep a good hole transport behavior. Also, the film absorption of PY1 generated a remarkable blue shift by about 50 nm relative to PY2, maintaining the undiminished extinction coefficient. It is believed that this blue-shifted absorption profile is helpful for NFOSCs with narrow band gap acceptors to harvest photons as much as possible and generate favorable photocurrent. Meanwhile, a deeper HOMO energy level by 0.26 eV was detected for PY1 relative to PY2 which is all-important for OSCs to gain a fair  $V_{OC}$ . Thus, a new structure wide band gap D-A polymer (PY1) with a deep HOMO energy level of -5.45 eV was obtained via the utilization of  $\pi$ -bridge fusion to the A moiety of D- $\pi$ -A polymer (PY2 or J50). The NFOSCs were fabricated with ITIC as the acceptor. The results reveal an all-round enhancement of photovoltaic parameters of  $V_{OC}$ ,  $J_{SC}$ , and FF as well as the PCE for PY1-based devices. The best PCE of PY1-based devices reaches 12.49%, with  $V_{OC}$  of 0.94 V,  $J_{SC}$  of 18.46 mA cm<sup>-2</sup>, and FF of 0.72, all of which significantly exceed those of PY2-optimal device with a PCE of 7.39%,  $V_{OC}$  of 0.77 V,  $J_{SC}$  of 14.54 mA cm<sup>-2</sup>, and FF of 0.66. Notably, the enhancement effectiveness via the  $\pi$ -bridge fusion even overmatches the fluorination of BTz-based-polymer J51 ( $V_{OC}$  of 0.82 V, PCE of 9.26%). Overall, we demonstrate an effective approach to tailor the optoelectronic properties of BTz-based photovoltaic materials and shed light on the design of new

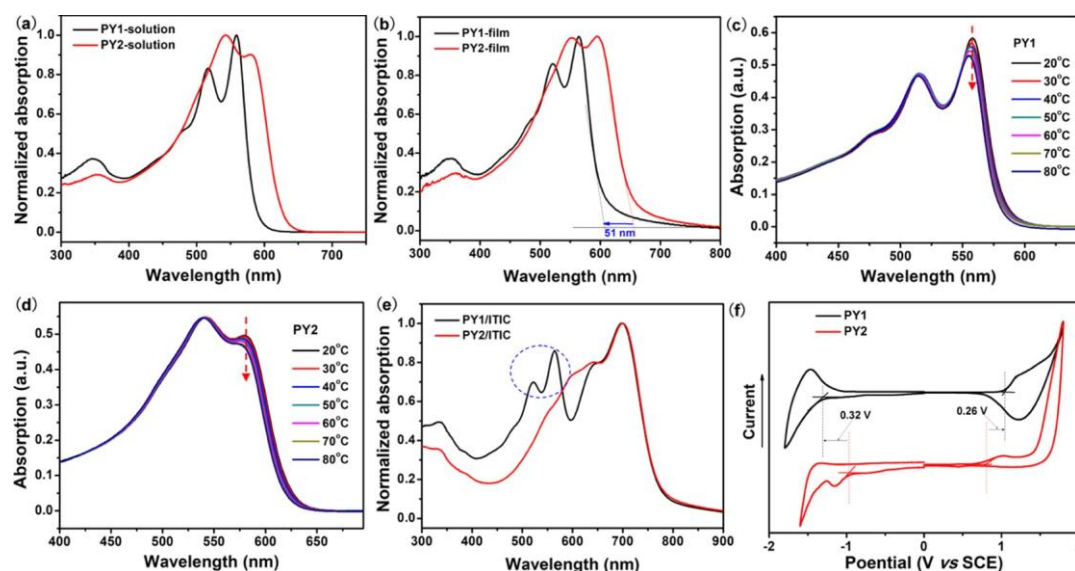


Figure 1. (a,b) UV-vis absorption spectra of PY1 and PY2 in CB solutions and as thin films. (c,d) Temperature-dependent absorption spectra of the two polymers in dilute CB solutions. (e) Blend films of PY1/ITIC and PY2/ITIC. (f) CV curves of two polymers.

Table 1. Thermal Stability, Molecular Weight, Optical Properties, and Energy Levels of Polymers

polymer	$T_d$ (°C)	$M_n$ (kDa)/PDI	$\lambda_{max}$ (nm)		$\epsilon^{film}$ ( $10^4 \text{ cm}^{-1}$ )	$E^{opt,d}$ (eV)	$\Phi_{ox}$ (V)	$\Phi_{red}$ (V)	HOMO <sup>b</sup> (eV)	LUMO <sup>b</sup> (eV)
			solution	film						
PY1	412	27.6/2.03	518, 559	520, 564	7.02	2.05	1.04	-1.29	-5.45	-3.12
PY2	391	30.8/2.29	543, 582	551, 597	6.99	1.89	0.78	-0.97	-5.19	-3.44

<sup>a</sup>Calculated from the onset wavelength of film absorption spectra. <sup>b</sup>Calculated from cyclic voltammograms curves.

class wide band gap conjugated polymers for efficient NFOSCs.

## RESULTS AND DISCUSSION

The synthetic routes and details of monomers 2BrDTBTz, 2Br fused-DTBTz, and the polymers PY1 and PY2 are given in the Supporting Information. The chemical structures of the monomers and intermediates were characterized by <sup>1</sup>H NMR and <sup>13</sup>C NMR spectroscopy. The polymers were synthesized by Stille polymerization with Pd(PPh<sub>3</sub>)<sub>4</sub> as the catalyst. Two polymers show good solubility in common solvent including chloroform, tetrahydrofuran, and chlorobenzene (CB) at room temperature. The number average molecular weights ( $M_n$ ) and polydispersity index (PDI) of PY1 and PY2, which were estimated by high-temperature gel permeation chromatography, were determined to be 27.6 and 30.8 kDa/2.29, respectively. The thermodynamic properties of the two polymers were determined by the thermogravimetric analysis (TGA). PY1 and PY2 show good thermal stability when the decomposition temperatures ( $T_d$ ) with 5% weight loss are 414 and 392 °C (see Figure S1).

The ultraviolet-visible (UV-vis) absorption spectra of PY1 and PY2 in dilute solutions and as thin films are shown in Figure 1, and the relevant data are summarized in Table 1. As displayed in Figure 1a,b, the weak bands around 350 nm should be attributed to the p-p\* transition for two polymers.<sup>34,35</sup> In the range of 450–650 nm, there are two distinct strong absorption peaks. Between them, the bands at the shorter wavelength probably originate from the intramolecular charge-transfer (ICT) effect, and the absorption characteristic at the longer wavelength was usually assigned as “aggregation peak” as previously reported, which is directly

correlated with the polymer aggregation in solution and crystallinity in the solid state.<sup>36–38</sup> Compared to PY2, PY1 keeps stronger intra- or/and intermolecular interactions with a sharp aggregation peak in the dilute solution. In going from solution to film, the aggregation peak of PY1 is still strong and the aggregation peak of PY2 is slightly raised relative to its solution state. The characteristic aggregation absorption peak is essential for effective molecular stacking and beneficial for the hole transport among the polymer backbones. To further evaluate the aggregation behaviors of two polymers, the temperature-dependent absorption spectra were measured in dilute CB solutions with the temperatures varying from 20 to 80 °C. As shown in Figure 1c, the aggregation peak of PY1 in solution is still evident and remarkably strong even heating at 80 °C. In contrast, the aggregation peak of PY2 was further weakened and becomes smooth in hot dilute solution (Figure 1d). Thus, we can roughly conclude that the intra- or/and intermolecular interactions of PY1 are superior to those of PY2. Another distinction lies in the apparent blue shift of absorption spectra from PY2 to PY1 in both solutions and films. Specifically, the film absorption onset of PY1 generates a significant blue shift by 51 nm relative to PY2, with both the ICT and aggregation peaks blue-shifted over 30 nm. Calculated from the onset wavelengths of film spectra, the optical band gaps were enlarged from 1.89 eV of PY2 to 2.05 eV of PY1. Thus, we built a wide band gap polymer via the fusion of  $\pi$ -bridge to A moiety, which could be disfavored in fullerene-based solar cells. However, considering the strong absorption of ITIC in the range of 600–750 nm, the avoidance of absorption in that wavelength range would afford a better complementation and broader photoresponse in polymer/ITIC BHJ blend. This can be observed more intuitively from

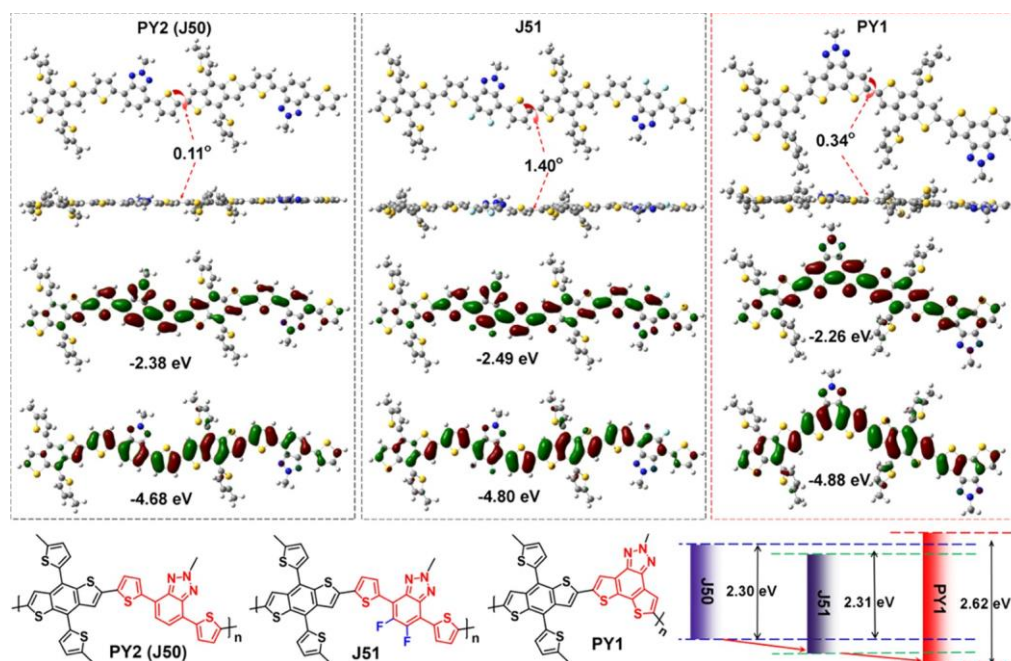


Figure 2. Molecular conformations, frontier energy levels of PY2 (J50), J51, and PY1 based on DFT calculations. From top to bottom: top view (dihedral angle), side view, electron cloud distributions of LUMO, and HOMO energy levels.

the absorption spectra of two BHJ blend films. As shown in Figure 1e, the two strong intrinsic peaks of PY1 can be detected obviously while those of PY2 were somewhat overlapped with ITIC. The expanded and stronger absorption of PY1/ITIC, as well as the stronger intermolecular interactions of PY1, could afford a more effective harvest of solar photons, contributing to the  $J_{SC}$  improvement of solar cells.

Electrochemical cyclic voltammetry (CV) measurements were performed to measure the oxidation/reduction potentials and estimate the energy levels of two polymers. The HOMO levels of polymers were calculated from their onset oxidation potential ( $\Phi_{ox}$ ). As shown in Figures 1f and S2, the  $\Phi_{ox}$  values of PY1 and PY2 were determined to be 1.04 and 0.78 V, corresponding to the HOMO energy levels of  $-5.45$  and  $-5.19$  eV, respectively. Likewise, the onset reduction potentials ( $\Phi_{red}$ ) of PY1 and PY2 were determined to be  $-1.29$  and  $-0.97$  V, corresponding to the lowest unoccupied molecular orbital (LUMO) energy levels of  $-3.12$  and  $-3.44$  eV, respectively. Thus, the fusion of  $\pi$ -bridge to the BTz unit could greatly downshift the HOMO energy level of the D–A polymer, beneficial for the promotion of  $V_{OC}$  of solar cells. The variation of electrochemical band gaps from PY1 to PY2 displays trends similar to their optical band gaps, both indicating the formation of wide band gap polymers after the  $\pi$ -bridge fusion.

As mentioned above, appropriate  $\pi$ -bridges are essential for most of D– $\pi$ –A polymers not only to adjust the basic photophysical/energy level properties but also play a role as a flexible transitional domain to mitigate the intense steric hindrance between the rigid D and A moieties. Thus, we performed the theoretical calculations of polymers PY2 (J50), PY1, and J51, with density functional theory (DFT) at the B3LYP/6-31G(d, p) level to evaluate the variation of the molecular conformations and further explore the shift of frontier energy levels before and after the  $\pi$ -bridge fusion as well as the fluorination of BTz unit. Before that, we calculated

the molecular conformations and frontier energy levels of two A units DTBTz and fused-DTBTz and collected the results in Figure S3. The long alkyl side chains were replaced by methyl groups to reduce the calculation time. Relative to DTBTz, the band gap of fused-DTBTz was expanded greatly with a deeper HOMO energy level and a higher LUMO energy level. This probably indicates that fused-DTBTz is a weaker A unit than DTBTz, which is essential to build wide band gap D–A conjugated polymers. Then, two repeat units of polymers were intercepted to perform the calculations. As shown in Figure 2, the dihedral angles between DTBTz and BDT moieties are negligible for PY2 or J50 ( $0.11^\circ$ ) and J51 ( $1.40^\circ$ ), suggesting the favorable planarity of polymer backbones. Gratifyingly, the  $\pi$ -bridge fusion to BTz does not trigger significant distortion for the resulting D–A polymer backbone, with a small dihedral angle ( $0.34^\circ$ ) between fused-DTBTz and BDT moieties. The decent planarity of the polymer backbone is essential for the efficient hole charge transport along the polymer backbone. Additionally, a decreased HOMO and increased LUMO energy levels of PY1 were concurrently detected compared to PY2 (J50), consistent with their CV measurements. Notably, the HOMO energy level of PY1 is even deeper than that of J51, indicating that the  $\pi$ -bridge fusion strategy is more effective than fluorination in the modulation of energy levels and could enable the OSCs with a higher  $V_{OC}$ . Again, the variation tendency of HOMO energy levels of PY1 and J51 are consistent with the experimental results.<sup>20</sup>

In order to evaluate the photovoltaic performance of polymer with  $\pi$ -bridge fusion structure, we fabricated OSCs with the conventional device architecture: ITO (indium tin oxide)/PEDOT:PSS/active layer/PDINO/Al. The detailed device fabrication processes are described in the Supporting Information. PY1 and PY2 were utilized as the donor materials, and nonfullerene ITIC was used as the acceptor material. The energy level diagram of materials in devices is shown in Figure 3. The device fabrication conditions including the donor/

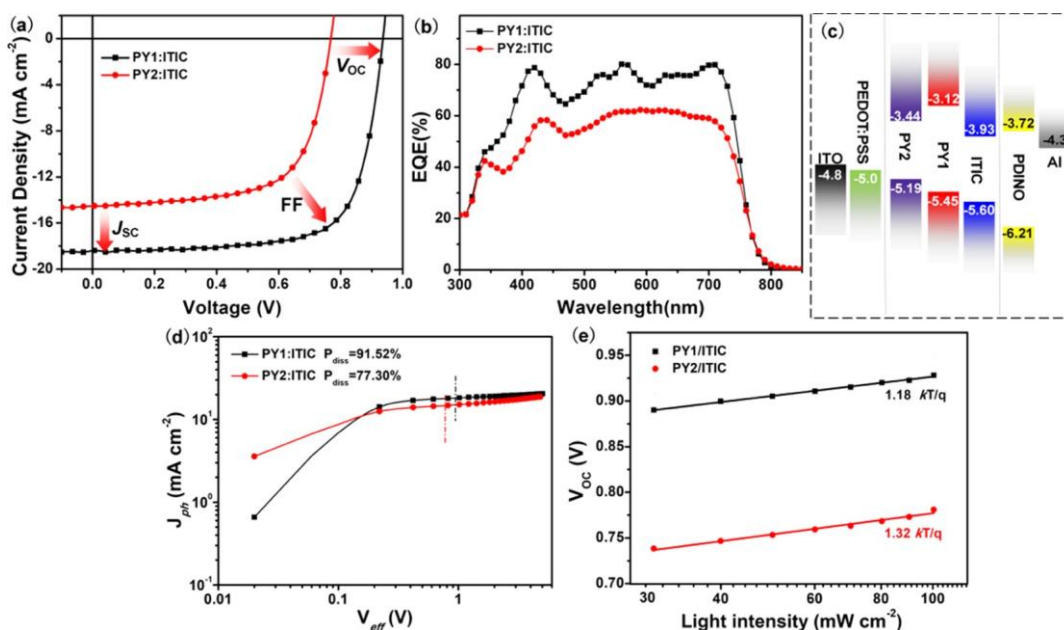


Figure 3. (a)  $J$ - $V$  curves of PY1- and PY2-based optimized OSCs. (b) Corresponding EQE spectra. (c) Energy level diagram of materials utilized in OSCs. (d)  $J_{ph}$  vs  $V_{eff}$  curves. (e)  $V_{OC}$ -Light intensity of two optimized OSCs.

Table 2. Device Parameters of OSCs Under the Illumination of AM 1.5G,  $100 \text{ mW cm}^{-2}$

polymer	$V_{OC}^a$ (V)	$J_{SC}^a$ ( $\text{mA cm}^{-2}$ )	FF <sup>a</sup>	PCE <sup>a</sup> (%) <sup>b</sup>	$\mu_h/\mu_e^b$ $10^{-4} \text{ cm}^2 \text{ V}^{-1} \text{ s}^{-1}$
PY1 <sup>c</sup>	0.94 (0.94 ± 0.005)	18.46 (18.22 ± 0.42)	0.72 (0.71 ± 0.01)	12.49 (12.20 ± 0.30)	4.87/3.13
PY2 <sup>c</sup>	0.77 (0.76 ± 0.01)	14.54 (14.23 ± 0.34)	0.66 (0.65 ± 0.01)	7.39 (7.19 ± 0.21)	1.73/2.90
J50 <sup>d</sup>	0.71 (0.71 ± 0.003)	12.93 (12.55 ± 0.24)	0.53 (0.51 ± 0.01)	4.80 (4.61 ± 0.11)	0.62/0.22
J51 <sup>d</sup>	0.82 (0.81 ± 0.008)	16.47 (16.33 ± 0.28)	0.69 (0.68 ± 0.01)	9.26 (9.07 ± 0.18)	4.32/3.74

<sup>a</sup>Average values with standard deviations were obtained from at least 10 cells. <sup>b</sup>Measured based on the SCLC model. <sup>c</sup>Thermal annealing at 130 °C for 10 min. <sup>d</sup>Extracted from the previous report.<sup>20</sup>

acceptor weight ratios, thickness of the active layer, and thermal annealing have been fully optimized. As shown in Table S1, the optimal weight ratios of PY1 and PY2 were determined to be 1:1 and 1:2, respectively, and the annealing treatment was essentially required for two devices.

The key device parameters of the best-performing OSCs are collected in Table 2 and the respective current density–voltage ( $J$ - $V$ ) curves are shown in Figure 3a. The OSCs fabricated from PY2/ITIC achieved its best PCE of 7.39%, with  $V_{OC}$  of 0.77 V,  $J_{SC}$  of  $14.54 \text{ mA cm}^{-2}$ , and FF of 0.66. The efficiency of PY2/ITIC is higher than the J50/ITIC system as reported originating from the proper side chain engineering of DTBTz and the resulting variation in charge transport behaviors. It's worth highlighting that an all-around improvement of the three key parameters was detected from PY1/ITIC devices. The OSCs of PY1/ITIC delivered the highest PCE up to 12.49% with a noticeably elevated  $V_{OC}$  of 0.94 V,  $J_{SC}$  of  $18.46 \text{ mA cm}^{-2}$ , and FF of 0.72, all of which are significantly higher than those of PY2/ITIC. The greatly boosted  $V_{OC}$  of the PY1-based device undoubtedly mainly originates from the deeper HOMO energy level than PY2 as depicted in CV measurements and theoretical calculations. The enhancement of the  $V_{OC}$  parameter is one focus of this design strategy ( $\pi$ -bridge fusion), given the inferior  $V_{OC}$  values often observed from DTBTz-based polymer fabricated devices. Additionally, one origination of the enhanced  $J_{SC}$  benefits from the better-matched absorption spectra of PY1 and ITIC as shown in Figure 1c and the raised external quantum efficiency (EQE)

spectra as shown in Figure 3b. The calculated integrated current densities ( $J_{SC}^{EQE}$ ) of two optimal devices from the EQE spectra are determined to be 17.54 and  $14.09 \text{ mA cm}^{-2}$ , slightly smaller than the recorded  $J_{SC}$  from the  $J$ - $V$  measurements with a deviation of about 5%. We note that the overall shape of EQE curves does not always follow the same trends with those of the absorption spectra of blend films, especially in the short wavelength between 300 and 500 nm. Apart from the absorption feature, the EQE response is also influenced by the BHJ morphologies, molecular orientations, charge transport, and recombination behaviors according to previous reports.<sup>39,40</sup> Moreover, most of the organic conjugated materials usually generate a stronger photoresponse in short wavelength range, accounting for the decent photoresponse of EQE curves in the UV range.

Furthermore, higher and balanced charge transport behaviors inside the BHJ blends could also enhance the photocurrent and FF of solar cells. The charge carrier mobilities of the two optimal BHJ blends were measured further by space-charge-limited current (SCLC) model. The hole and electron mobilities are summarized in Table 2, and the plots of the current density versus voltage of hole-only and electron-only devices are displayed in Figures S4 and S5. Similar electron mobilities ( $\mu_e$ ) inside PY1/ITIC and PY2/ITIC were determined to be  $3.13 \times 10^{-4}$  and  $2.90 \times 10^{-4} \text{ cm}^2 \text{ V}^{-1} \text{ s}^{-1}$ , respectively. Inspiringly, more efficient hole charge transport exists in PY1/ITIC based device with the hole mobility ( $\mu_h$ ) up to  $4.87 \times 10^{-4} \text{ cm}^2 \text{ V}^{-1} \text{ s}^{-1}$ , over 2.5 folds than that of PY2/

ITIC ( $1.73 \times 10^{-4} \text{ cm}^2 \text{ V}^{-1} \text{ s}^{-1}$ ) and should mainly profit from the superior properties of polymeric donor PY1. The greatly improved hole mobility and consequent more balanced hole/electron charge transport of PY1/ITIC-based devices positively contribute to the higher EQE response, more competitive  $J_{\text{SC}}$ , and FF as well as PCEs than PY2/ITIC devices. Dramatically, as evident from Table 2, PY1-based devices demonstrate elevated  $V_{\text{OC}}$  values by 0.12 V than the devices of classical polymer J51 with fluorinated BTz unit. Relative to PY2, J50, and J51, the all-around raised key photovoltaic parameters as well as PCEs of PY1 fabricated OSCs indicate that the  $\pi$ -fusion strategy is a more efficient approach than the traditional D- $\pi$ -A analog polymer backbone and even the fluorination strategy of BTz-based polymers in NFOSCs. Combined with the further side chain engineering or fluorination in fused-DTBTz (A) or/and the electron-rich BDT (D) moiety, more efficient OSCs could be expected from the fused-DTBTz moiety-based wide band gap D-A conjugated polymers.

To gain a deep insight into the charge generation and dissociation behaviors inside BHJ OSCs, we measured the plots of photocurrent ( $J_{\text{ph}}$ ) versus effective voltage ( $V_{\text{eff}}$ ) as displayed in Figure 3d. The parameter definitions are described in the Supporting Information. The exciton dissociation probability [ $P_{\text{diss}}(E, T)$ ], which is correlated with the electric field ( $E$ ) and temperature ( $T$ ), is determined from the ratio of  $J_{\text{ph}}/J_{\text{sat}}$  (saturation current).<sup>41,42</sup> The  $P_{\text{diss}}(E, T)$  of two devices are calculated to be 91.52 and 77.30%, respectively, under their short-circuit conditions ( $V_{\text{eff}} = V_{\text{OC}}$ ). The low  $P_{\text{diss}}(E, T)$  of the PY2-based device suggests that only three-quarters of the total photogenerated excitons was dissociated into free hole and electron charges, and one-quarter of the excitons was annihilated, even displaying strong blend absorption spectra and higher value around 600 nm than PY1/ITIC. The much greater  $P_{\text{diss}}(E, T)$  of the PY1-based device indicates that higher exciton dissociation and charge extraction efficiencies were generated, which is well in agreement with the superior EQE response and higher performance of OSCs. Moreover, the correlation of  $V_{\text{OC}}$  with the light intensity was measured to evaluate the degree of recombination inside OSCs. Figure 3e shows the semilogarithmic plot of  $V_{\text{OC}}$  as a function of the light intensity, and the parameter definitions are presented in the Supporting Information. Slopes of 1.18 and 1.32  $kT/q$  (where  $k$  is the Boltzmann constant,  $T$  is the temperature, and  $q$  is the elementary charge) were calculated from PY1- and PY2-based solar cells. This suggests that considerable trap-assisted recombination was involved inside the device of PY2/ITIC, and recombination of free carriers was to some extent suppressed inside the device of PY1/ITIC under the open-circuit condition.<sup>43,44</sup>

The detailed BHJ morphologies of the two blend films were investigated by atomic force microscope (AFM) and transmission electron microscope (TEM) measurements. As shown in Figure 4a,b, the two optimal BHJ blend films of PY1/ITIC and PY2/ITIC exhibit semblable nanoscale surface morphology characteristics with a similar and moderate root mean square surface roughness of 3.53 and 3.87 nm, respectively. However, there are still some distinct microstructures detected from their internal morphologies based on the measurement of TEM. As depicted in Figure 4c,d, the PY1/ITIC-fabricated BHJ film reveals a more uniform morphology featured with a smaller nanoscale phase-separation characteristic than PY2/ITIC blend films. This finely dispersed inner morphology of BHJ blends is known to be more favorable for effective exciton

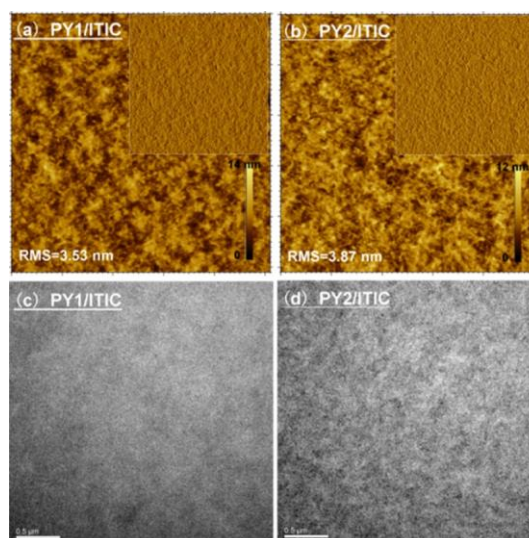


Figure 4. (a) AFM height images of the optimal PY1/ITIC and (b) PY2/ITIC blend films ( $5 \times 5 \mu\text{m}$ ). The inset is the respective phase image; (c) TEM image of the optimal PY1/ITIC and (d) PY2/ITIC blend films (the scale bar is  $0.5 \mu\text{m}$ ).

diffusion, charge separation, and transport, affording enhanced free carrier mobilities and suppressed charge recombination as discovered above.<sup>45</sup>

In order to discover the correlation between the polymer structures and molecular stacking orientations of two polymers, grazing incidence wide angle X-ray scattering (GIWAXS) was implemented on the pure films of PY1 and PY2. As displayed in Figure 5a–c, two polymers reveal predominant face-on orientations, with sharp (010)  $\pi$ - $\pi$  diffraction peaks mainly observed in the out-of-plane (OOP) direction and (100) lamellar stacking located in in-plane (IP) direction. This indicates that minimal disturbance was produced as for the molecular orientations after the  $\pi$ -bridge fusion to A moiety of D- $\pi$ -A conjugated polymer. However, some minor transformations were detected related to the intensity and molecular stacking spacing of two polymers. Both the  $\pi$ - $\pi$  stacking in OOP direction and lamellar stacking in IP direction of PY1 are mildly enhanced relative to PY2, accompanying with the slightly increased stacking distances ( $d_{\text{spacing}}$ ). In going from PY1 to PY2, the  $d_{\text{spacing}}$  of face-on orientation is enlarged from 3.60 to 3.69 Å, along with the  $d_{\text{spacing}}$  of lamellar stacking in IP direction enlarged from 22.4 to 24.8 Å. The variation of molecular stacking distances is probably induced by the transformation of polymer structures. However, the maintained and stronger face-on orientations of PY1 is positive, considering the realized significant optimization of HOMO energy level and absorption feature corresponding to the great improvement of  $V_{\text{OC}}$  and  $J_{\text{SC}}$  of solar cells. Moreover, the molecular stacking orientations of two optimal BHJ blend films of PY1/ITIC and PY2/ITIC keep the apparent nature similar to those of two polymers. As displayed in Figure 5d–f, in going from PY1/ITIC to PY2/ITIC, the  $d_{\text{spacing}}$  of face-on orientations and lamellar stacking orientations are broadened from 3.55 to 3.63 Å and from 20.0 to 22.6 Å, respectively. However, the stacking intensities in two BHJ blends are slightly different. Compared to PY2/ITIC, the intensities of face-on orientations and lamellar stacking orientations of PY1/ITIC have moderate enhancement by about 1.26 and 1.30 folds, respectively, which should be more beneficial for the

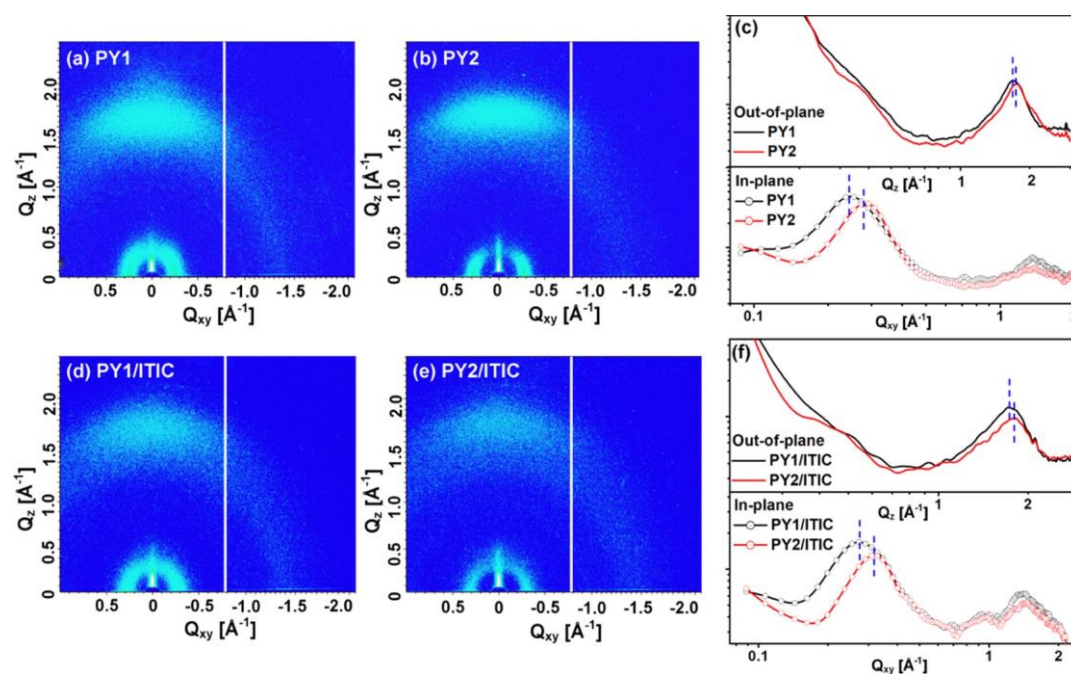


Figure 5. GIWAXS scattering patterns of pure polymer films of (a) PY1 and (b) PY2, and (c) their corresponding line profiles. GIWAXS scattering patterns of blend films of (d) PY1/ITIC and (e) PY2/ITIC and (f) their corresponding line profiles.

efficient charge transport in BHJ blends and consistent with the improved hole mobility and balanced hole/electron mobilities detected in PY1/ITIC blends.<sup>46,47</sup> Overall, from the results of GIWAXS studies of two neat polymers and two BHJ blend films, we can discover that the distances of molecular stacking are slightly enlarged after the  $\pi$ -bridge fusion strategy which is negative for the charge transport along the polymer backbones or among the polymer chains. However, the slightly enhanced molecular packing especially the favorable face-on orientations somewhat covered the deficiency and promoted the overall charge transport behaviors.

## CONCLUSIONS

In conclusion, we proposed a significant strategy to design a new structure wide band gap D–A polymer appropriate for high-performance NFOSCs. That is, the classical D– $\pi$ –A polymer was evolved into a new D–A polymer through the fusion of  $\pi$ -bridge into the A moiety. Specifically, the thiophene  $\pi$ -bridge of BDT– $\pi$ –BTz-based polymer PY2 (analog of reported J50) was incorporated into the A moiety BTz and produced a novel structure D–A polymer PY1 with fused-DTBTz as the new A moiety. The results witness a largely decreased HOMO energy level of PY1 by 0.26 eV, accompanying with the significantly blue-shifted absorption spectrum with the optical band gap expanded from 1.89 eV (PY2) to 2.05 eV (PY1). The NFOSCs with ITIC as the acceptor were fabricated. Beneficial from the deeper HOMO energy level of PY1, obviously enhanced  $V_{OC}$  from 0.77 V of PY2:ITIC to 0.94 V of PY1:ITIC was recorded. It's known that the D– $\pi$ –A polymers based on BTz and even fluorinated-BTz units usually suffered from inferior  $V_{OC}$  values and this  $\pi$ -bridge fusion strategy assuredly solved this dilemma. Moreover, relative to PY2, the visibly blue-shifted absorption of PY1 afforded better complementation and a broader photoresponse with ITIC, which helps to deliver the increased  $J_{SC}$  of PY1-

based solar cells. Additionally, mildly stronger face-on molecular stacking orientations were observed both in PY1 and PY1/ITIC blend films, in spite of the slightly broadened packing distances. The eventually offsetting influence of the molecular stacking feature generated an overall promotion in charge transport inside devices and partly contributed to the raised  $J_{SC}$  and FF of OSCs. Thus, an all-round enhancement of photovoltaic parameters of  $V_{OC}$ ,  $J_{SC}$ , FF as well as the PCE was detected from PY1-based devices. The best efficiency of PY1-based devices reaches 12.49%, with a  $V_{OC}$  of 0.94 V,  $J_{SC}$  of 18.46 mA cm<sup>-2</sup>, and FF of 0.72, significantly overmatching those of the PY2-based optimal device with a PCE of 7.39%,  $V_{OC}$  of 0.77 V,  $J_{SC}$  of 14.54 mA cm<sup>-2</sup>, and FF of 0.66, and even the reported fluorination of BTz-based polymer J51 ( $V_{OC}$  of 0.82 V, PCE of 9.26%). Hence, we reported a new strategy for the design of efficient wide band gap D–A conjugated polymers in this work. Hopefully, there is still a huge margin for improvement to reach the state-of-the-art efficiencies with rational fluorination or chlorination of the fused-DTBTz unit or the D moiety of the D–A polymers.

## EXPERIMENTAL SECTION

**Materials.** All reagents and chemicals were purchased from TCI Co., Sigma-Aldrich Co., and Alfa Aesar Co. and were used without further purification unless otherwise stated. The acceptor material ITIC was purchased from Derthon Co. The synthesis details of monomers 2BrDTBTz and 2Br fused-DTBTz and two polymers PY1 and PY2 were collected in the Supporting Information.

## ASSOCIATED CONTENT

### Supporting Information

The Supporting Information is available free of charge on the ACS Publications website at DOI: 10.1021/acsami.9b09486.

Materials characterization techniques, device fabrication procedures, synthetic details of polymers, TGA studies, characterizations of the polymer solar cells, and DFT studies and hole/electron mobility studies (PDF).

## AUTHOR INFORMATION

## Corresponding Authors

\*E-mail: liyh@qibebt.ac.cn (Y. L.).

\*E-mail: zhengn@scut.edu.cn (N. Z.).

\*E-mail: mlsun@ouc.edu.cn (M. S.).

\*E-mail: yangrq@qibebt.ac.cn (R. Y.).

ORCID 

Yonghai Li: 0000-0002-5748-0258

Shuguang Wen: 0000-0001-9181-9019

Mingliang Sun: 0000-0002-6245-3844

Renqiang Yang: 0000-0001-6794-7416

## Author Contributions

L.Y. and Y.L. contributed equally. The manuscript was written through contributions of all authors. All authors have given approval to the final version of the manuscript.

## Notes

The authors declare no competing financial interest.

## ACKNOWLEDGMENTS

The authors are deeply grateful to the National Natural Science Foundation of China (21502205, 51573205, 51773220), the Ministry of Science and Technology of China (2016YFE0115000), Qingdao Source Innovation Plan Applied Basic Research Project (18-2-2-28-jch) and DICP&QIBEBT (UN201805) for the financial support. The work was also supported by Dalian National Laboratory For Clean Energy (DNL), CAS. The authors appreciate the help of Raji for the paper correction.

## REFERENCES

- (1) Yu, G.; Gao, J.; Hummelen, J. C.; Wudl, F.; Heeger, A. J. Polymer Photovoltaic Cells: Enhanced Efficiencies via a Network of Internal Donor-Acceptor Heterojunctions. *Science* 1995, 270, 1789–1791.
- (2) Xiao, Z.; Jia, X.; Ding, L. Ternary Organic Solar Cells Offer 14% Power Conversion Efficiency. *Sci. Bull.* 2017, 62, 1562–1564.
- (3) Li, G.; Shrotriya, V.; Huang, J.; Yao, Y.; Moriarty, T.; Emery, K.; Yang, Y. High-Efficiency Solution Processable Polymer Photovoltaic Cells by Self-Organization of Polymer Blends. *Nat. Mater.* 2005, 4, 864–868.
- (4) Holliday, S.; Ashraf, R. S.; Nielsen, C. B.; Kirkus, M.; Röhr, J. A.; Tan, C.-H.; Collado-Fregoso, E.; Knall, A.-C.; Durrant, J. R.; Nelson, J.; McCulloch, I. A Rhodanine Flanked Nonfullerene Acceptor for Solution-Processed Organic Photovoltaics. *J. Am. Chem. Soc.* 2015, 137, 898–904.
- (5) Li, Y.; Yang, Y.; Bao, X.; Qiu, M.; Liu, Z.; Wang, N.; Zhang, G.; Yang, R.; Zhang, D. New  $\pi$ -Conjugated Polymers as Acceptors Designed for All Polymer Solar Cells Based on Imide/Amide-Derivatives. *J. Mater. Chem. C* 2016, 4, 185–192.
- (6) McAfee, S. M.; Topple, J. M.; Hill, I. G.; Welch, G. C. Key Components to the Recent Performance Increases of Solution Processed Non-Fullerene Small Molecule Acceptors. *J. Mater. Chem. A* 2015, 3, 16393–16408.
- (7) Zhao, J.; Li, Y.; Yang, G.; Jiang, K.; Lin, H.; Ade, H.; Ma, W.; Yan, H. Efficient Organic Solar Cells Processed from Hydrocarbon Solvents. *Nat. Energy* 2016, 1, 15027.
- (8) Liang, Y.; Xu, Z.; Xia, J.; Tsai, S.-T.; Wu, Y.; Li, G.; Ray, C.; Yu, L. For the Bright Future of Bulk Heterojunction Polymer Solar Cells with Power Conversion Efficiency of 7.4%. *Adv. Mater.* 2010, 22, E135–E138.
- (9) Chen, J.-D.; Cui, C.; Li, Y.; Zhou, L.; Ou, Q.; Li, C.; Li, Y.; Tang, J. Single-Junction Polymer Solar Cells Exceeding 10% Power Conversion Efficiency. *Adv. Mater.* 2015, 27, 1035–1041.
- (10) Vohra, V.; Kawashima, K.; Kakara, T.; Koganezawa, T.; Osaka, I.; Takimiya, K.; Murata, H. Efficient Inverted Polymer Solar Cells Employing Favourable Molecular Orientation. *Nat. Photonics* 2015, 9, 403–408.
- (11) Dey, S. Recent Progress in Molecular Design of Fused Ring Electron Acceptors for Organic Solar Cells. *Small* 2019, 15, 1900134.
- (12) Liu, T.; Luo, Z.; Fan, Q.; Zhang, G.; Zhang, L.; Gao, W.; Guo, X.; Ma, W.; Zhang, M.; Yang, C.; Li, Y.; Yan, H. Use of Two Structurally Similar Small Molecular Acceptors Enabling Ternary Organic Solar Cells with High Efficiencies and Fill Factors. *Energy Environ. Sci.* 2018, 11, 3275–3282.
- (13) Zhang, H.; Yao, H.; Hou, J.; Zhu, J.; Zhang, J.; Li, W.; Yu, R.; Gao, B.; Zhang, S.; Hou, J. Over 14% Efficiency in Organic Solar Cells Enabled by Chlorinated Nonfullerene Small-Molecule Acceptors. *Adv. Mater.* 2018, 30, 1800613.
- (14) Li, Y.; Zheng, N.; Yu, L.; Wen, S.; Gao, C.; Sun, M.; Yang, R. A Simple Phenyl Group Introduced at the Tail of Alkyl Side Chains of Small Molecular Acceptors: New Strategy to Balance the Crystallinity of Acceptors and Miscibility of Bulk Heterojunction Enabling Highly Efficient Organic Solar Cells. *Adv. Mater.* 2019, 31, 1807832.
- (15) Yuan, J.; Zhang, Y.; Zhou, L.; Zhang, G.; Yip, H.-L.; Lau, T.-K.; Lu, X.; Zhu, C.; Peng, H.; Johnson, P. A.; Leclerc, M.; Cao, Y.; Ulanski, J.; Li, Y.; Zou, Y. Single-Junction Organic Solar Cell with over 15% Efficiency Using Fused-Ring Acceptor with Electron-Deficient Core. *Joule* 2019, 3, 1140–1151.
- (16) Yuan, J.; Zhang, Y.; Zhou, L.; Zhang, C.; Lau, T. K.; Zhang, G.; Lu, X.; Yip, H. L.; So, S. K.; Beaupre, S.; Mainville, M.; Johnson, P. A.; Leclerc, M.; Chen, H.; Peng, H.; Li, Y.; Zou, Y. Fused Benzothiadiazole: A Building Block for n-Type Organic Acceptor to Achieve High-Performance Organic Solar Cells. *Adv. Mater.* 2019, 31, 1807577.
- (17) Meng, L.; Zhang, Y.; Wan, X.; Li, C.; Zhang, X.; Wang, Y.; Ke, X.; Xiao, Z.; Ding, L.; Xia, R.; Yip, H.; Cao, Y.; Chen, Y. Organic and Solution-Processed Tandem Solar Cells with 17.3% Efficiency. *Science* 2018, 361, 1094–1098.
- (18) Ma, Y.; Zhang, M.; Yan, Y.; Xin, J.; Wang, T.; Ma, W.; Tang, C.; Zheng, Q. Ladder-Type Dithienonaphthalene-Based Small-Molecule Acceptors for Efficient Nonfullerene Organic Solar Cells. *Chem. Mater.* 2017, 29, 7942–7952.
- (19) Che, X.; Li, Y.; Qu, Y.; Forrest, S. R. High Fabrication Yield Organic Tandem Photovoltaics Combining Vacuum- and Solution-Processed Subcells with 15% Efficiency. *Nat. Energy* 2018, 3, 422–427.
- (20) Gao, L.; Zhang, Z.-G.; Bin, H.; Xue, L.; Yang, Y.; Wang, C.; Liu, F.; Russell, T. P.; Li, Y. High-Efficiency Nonfullerene Polymer Solar Cells with Medium Bandgap Polymer Donor and Narrow Bandgap Organic Semiconductor Acceptor. *Adv. Mater.* 2016, 28, 8288–8295.
- (21) Gao, L.; Zhang, Z. G.; Xue, L.; Min, J.; Zhang, J.; Wei, Z.; Li, Y. All-Polymer Solar Cells Based on Absorption-Complementary Polymer Donor and Acceptor with High Power Conversion Efficiency of 8.27%. *Adv. Mater.* 2016, 28, 1884–1890.
- (22) Chen, W.; Huang, G.; Li, X.; Wang, H.; Li, Y.; Jiang, H.; Zheng, N.; Yang, R. Side-Chain-Promoted Benzodithiophene-based Conjugated Polymers toward Striking Enhancement of Photovoltaic Properties for Polymer Solar Cells. *ACS Appl. Mater. Interfaces* 2018, 10, 42747–42755.
- (23) Xue, L.; Yang, Y.; Xu, J.; Zhang, C.; Bin, H.; Zhang, Z.-G.; Qiu, B.; Li, X.; Sun, C.; Gao, L.; Yao, J.; Chen, X.; Yang, Y.; Xiao, M.; Li, Y. Side Chain Engineering on Medium Bandgap Copolymers to Suppress Triplet Formation for High-Efficiency Polymer Solar Cells. *Adv. Mater.* 2017, 29, 1703344.
- (24) Bin, H.; Yang, Y.; Peng, Z.; Ye, L.; Yao, J.; Zhong, L.; Sun, C.; Gao, L.; Huang, H.; Li, X.; Qiu, B.; Xue, L.; Zhang, Z.-G.; Ade, H.; Li, Y. Effect of Alkylsilyl Side-Chain Structure on Photovoltaic Properties of Conjugated Polymer Donors. *Adv. Energy Mater.* 2017, 8, 1702324.
- (25) He, D.; Zhao, F.; Xin, J.; Rech, J. J.; Wei, Z.; Ma, W.; You, W.; Li, B.; Jiang, L.; Li, Y.; Wang, C. A Fused Ring Electron Acceptor with Decacyclic Core Enables over 13.5% Efficiency for Organic Solar Cells. *Adv. Energy Mater.* 2018, 8, 1802050.



- (26) Li, W.; Albrecht, S.; Yang, L.; Roland, S.; Tumbleston, J. R.; McAfee, T.; Yan, L.; Kelly, M. A.; Ade, H.; Neher, D.; You, W. Mobility-Controlled Performance of Thick Solar Cells Based on Fluorinated Copolymers. *J. Am. Chem. Soc.* 2014, **136**, 15566–15576.
- (27) Li, Y.; Wang, J.; Liu, Y.; Qiu, M.; Wen, S.; Bao, X.; Wang, N.; Sun, M.; Yang, R. Investigation of Fluorination on Donor Moiety of Donor-Acceptor 4,7-Dithienylbenzothiadiazole-Based Conjugated Polymers toward Enhanced Photovoltaic Efficiency. *ACS Appl. Mater. Interfaces* 2016, **8**, 26152–26161.
- (28) Liu, D.; Zhao, W.; Zhang, S.; Ye, L.; Zheng, Z.; Cui, Y.; Chen, Y.; Hou, J. Highly Efficient Photovoltaic Polymers Based on Benzodithiophene and Quinoxaline with Deeper HOMO Levels. *Macromolecules* 2015, **48**, 5172–5178.
- (29) Wolf, J.; Cruciani, F.; Labban, A.; Beaujuge, P. M. Wide Band-Gap 3,4-Difluorothiophene-Based Polymer with 7% Solar Cell Efficiency: An Alternative to P3HT. *Chem. Mater.* 2015, **27**, 4184–4187.
- (30) Zaborova, E.; Cházec, P.; Bechara, R.; Lécaque, P.; Heiser, T.; Mery, S.; Leclerc, N. Thiazole as a Weak Electron-Donor Unit to Lower the Frontier Orbital Energy Levels of Donor-Acceptor Alternating Conjugated Materials. *Chem. Commun.* 2013, **49**, 9938–9940.
- (31) Duan, C.; van Franeker, J. J.; Wienk, M. M.; Janssen, R. A. J. High Open Circuit Voltage Polymer Solar Cells Enabled by Employing Thiazoles in Semiconducting Polymers. *Polym. Chem.* 2016, **7**, 5730–5738.
- (32) Zhu, D.; Bao, X.; Zhu, Q.; Gu, C.; Qiu, M.; Wen, S.; Wang, J.; Shahid, B.; Yang, R. Thienothiophene-based Copolymers for High-Performance Solar Cells, Employing Different Orientations of the Thiazole Group as a  $\pi$  Bridge. *Energy Environ. Sci.* 2017, **10**, 614–620.
- (33) Arroyave, F. A.; Richard, C. A.; Reynolds, J. R. Efficient Synthesis of Benzo[1,2-b:6,5-b']dithiophene-4,5-dione (BDTD) and Its Chemical Transformations into Precursors for  $\pi$ -Conjugated Materials. *Org. Lett.* 2012, **14**, 6138–6141.
- (34) Li, K.; Li, Z.; Feng, K.; Xu, X.; Wang, L.; Peng, Q. Development of Large Band-Gap Conjugated Copolymers for Efficient Regular Single and Tandem Organic Solar Cells. *J. Am. Chem. Soc.* 2013, **135**, 13549–13557.
- (35) Li, Y.; Liu, D.; Wang, J.; Zhang, Z.-G.; Li, Y.; Liu, Y.; Zhu, T.; Bao, X.; Sun, M.; Yang, R. Crystalline Medium-Bandgap Light-Harvesting Donor Material Based on  $\beta$ -Naphthalene Asymmetric-Modified Benzodithiophene Moiety toward Efficient Polymer Solar Cells. *Chem. Mater.* 2017, **29**, 8249–8257.
- (36) Li, Y.; Zhang, G.; Liu, Z.; Chen, X.; Wang, J.; Di, C. a.; Zhang, D. Alternating Electron Donor-Acceptor Conjugated Polymers Based on Modified Naphthalene Diimide Framework: The Large Enhancement of p-Type Semiconducting Performance upon Solvent Vapor Annealing. *Macromolecules* 2013, **46**, 5504–5511.
- (37) Wang, Z.; Li, Z.; Liu, J.; Mei, J.; Li, K.; Li, Y.; Peng, Q. Solution-Processable Small Molecules for High-Performance Organic Solar Cells with Rigidly Fluorinated 2, 2'-Bithiophene Central Cores. *ACS Appl. Mater. Interfaces* 2016, **8**, 11639–11648.
- (38) Ashraf, R. S.; Schroeder, B. C.; Bronstein, H. A.; Huang, Z.; Thomas, S.; Kline, R. J.; Brabec, C. J.; Rannou, P.; Anthopoulos, T. D.; Durrant, J. R.; McCulloch, I. The Influence of Polymer Purification on Photovoltaic Device Performance of a Series of Indacenodithiophene Donor Polymers. *Adv. Mater.* 2013, **25**, 2029–2034.
- (39) Ye, L.; Jiao, X.; Zhang, S.; Yao, H.; Qin, Y.; Ade, H.; Hou, J. Control of Mesoscale Morphology and Photovoltaic Performance in Diketopyrrolopyrrole-Based Small Band Gap Terpolymers. *Adv. Energy Mater.* 2016, **7**, 1601138.
- (40) Ye, L.; Zhang, S.; Ma, W.; Fan, B.; Guo, X.; Huang, Y.; Ade, H.; Hou, J. From Binary to Ternary Solvent: Morphology Fine-Tuning of D/A Blends in PDPP3T-based Polymer Solar Cells. *Adv. Mater.* 2012, **24**, 6335–6341.
- (41) Wu, J.-L.; Chen, F.-C.; Hsiao, Y.-S.; Chien, F.-C.; Chen, P.; Kuo, C.-H.; Huang, M. H.; Hsu, C.-S. Surface Plasmonic Effects of Metallic Nanoparticles on the Performance of Polymer Bulk Heterojunction Solar Cells. *ACS Nano* 2011, **5**, 959–967.
- (42) Shrotriya, V.; Yao, Y.; Li, G.; Yang, Y. Effect of Self-Organization in Polymer/Fullerene Bulk Heterojunctions on Solar Cell Performance. *Appl. Phys. Lett.* 2006, **89**, 063505.
- (43) Zhang, G.; Xu, X.; Bi, Z.; Ma, W.; Tang, D.; Li, Y.; Peng, Q. Fluorinated and Alkylthiolated Polymeric Donors Enable both Efficient Fullerene and Nonfullerene Polymer Solar Cells. *Adv. Funct. Mater.* 2018, **28**, 1706404.
- (44) Kyaw, A. K. K.; Wang, D. H.; Wynands, D.; Zhang, J.; Nguyen, T.-Q.; Bazan, G. C.; Heeger, A. J. Improved Light Harvesting and Improved Efficiency by Insertion of an Optical Spacer (ZnO) in Solution-Processed Small-Molecule Solar Cells. *Nano Lett.* 2013, **13**, 3796–3801.
- (45) Park, G. E.; Choi, S.; Park, S. Y.; Lee, D. H.; Cho, M. J.; Choi, D. H. Eco-Friendly Solvent-Processed Fullerene-Free Polymer Solar Cells with over 9.7% Efficiency and Long-Term Performance Stability. *Adv. Energy Mater.* 2017, **7**, 1700566.
- (46) Liu, Y.; Li, M.; Zhou, X.; Jia, Q.-Q.; Feng, S.; Jiang, P.; Xu, X.; Ma, W.; Li, H.-B.; Bo, Z. Nonfullerene Acceptors with Enhanced Solubility and Ordered Packing for High-Efficiency Polymer Solar Cells. *ACS Energy Lett.* 2018, **3**, 1832–1839.
- (47) Jeon, S. J.; Han, Y. W.; Moon, D. K. Drastic Changes in Properties of Donor-Acceptor Polymers Induced by Asymmetric Structural Isomers for Application to Polymer Solar Cells. *ACS Appl. Mater. Interfaces* 2019, **11**, 9239–9250.